AFRL-AFOSR-UK-TR-2019-0056

An adaptive numerical methodology for mesoscale binder-crystal interactions and damage propagation in impact loaded energetic materials

Nikica Petrinic
THE UNIVERSITY OF OXFORD
UNIVERSITY OFFICES
OXFORD, OX1 2JD
GB

11/13/2019
Final Report

Air Force Research Laboratory
Air Force Office of Scientific Research
European Office of Aerospace Research and Development
Unit 4515 Box 14, APO AE 09421

REPORT DOCUMENTATION PAGE

Form Approved
OMB No. 0704-0188

1. REPORT DATE *(DD-MM-YYYY)*	2. REPORT TYPE	3. DATES COVERED *(From - To)*
13-11-2019	Final	15 Dec 2016 to 14 Jun 2017

4. TITLE AND SUBTITLE
An adaptive numerical methodology for mesoscale binder-crystal interactions and damage propagation in impact loaded energetic materials

5a. CONTRACT NUMBER

5b. GRANT NUMBER
FA9550-17-1-0618

5c. PROGRAM ELEMENT NUMBER
61102F

6. AUTHOR(S)
Nikica Petrinic

5d. PROJECT NUMBER

5e. TASK NUMBER

5f. WORK UNIT NUMBER

7. PERFORMING ORGANIZATION NAME(S) AND ADDRESS(ES)
THE UNIVERSITY OF OXFORD
UNIVERSITY OFFICES
OXFORD, OX1 2JD GB

8. PERFORMING ORGANIZATION REPORT NUMBER

9. SPONSORING/MONITORING AGENCY NAME(S) AND ADDRESS(ES)
EOARD
Unit 4515
APO AE 09421-4515

10. SPONSOR/MONITOR'S ACRONYM(S)
AFRL/AFOSR IOE

11. SPONSOR/MONITOR'S REPORT NUMBER(S)
AFRL-AFOSR-UK-TR-2019-0056

12. DISTRIBUTION/AVAILABILITY STATEMENT
A DISTRIBUTION UNLIMITED: PB Public Release

13. SUPPLEMENTARY NOTES

14. ABSTRACT
The ability to model the stress concentration, strain localization, crack initiation and propagation at mesoscopic length scales of heterogeneous materials such as polymer bonded explosives is critical to preventing undesirable ignitions. The research conducted in this study addresses the ability to model the strain localization, crack initiation and propagation by using explicit Lagrangian solution of the underlying partial differential equations within domains of interest discretized using finite elements and initially rigid cohesive elements. This approach is superior in its ability to model stress wave propagation excited by rapidly applied loads along model boundaries as it does not suffer from inaccuracies imposed by numerically generated internal impedance boundaries to their propagation. New criteria for detection of the onset of strain localisation, new algorithms for activation of initially rigid cohesive elements, strain softening, crack initiation and crack propagation have been implemented within in-house software DEST (Discrete Elements Simulation Tools) in order to enable existing and new experimental data to be used to enable further improvements of both the understanding of the underlying physical process as well as thus motivated further improvements of related modelling capabilities. The developed algorithms are presented alongside benchmarks which confirm their effectiveness.

15. SUBJECT TERMS
EOARD, Energetic materials, Cohesive zone model, Polymer composite, Polymer bonded explosives

16. SECURITY CLASSIFICATION OF:			17. LIMITATION OF ABSTRACT	18. NUMBER OF PAGES	19a. NAME OF RESPONSIBLE PERSON
a. REPORT	b. ABSTRACT	c. THIS PAGE			FOLEY, JASON
Unclassified	Unclassified	Unclassified	SAR		19b. TELEPHONE NUMBER *(Include area code)* 011-44-1895-616036

Standard Form 298 (Rev. 8/98)
Prescribed by ANSI Std. Z39.18

UNIVERSITY OF OXFORD
DEPARTMENT OF ENGINEERING SCIENCE
SOLID MECHANICS AND MATERIALS ENGINEERING GROUP
IMPACT ENGINEERING LABORATORY

Project reference: EOARD grant #FA9550-17-1-0618	**Report No.** SMG107a
Project title: Mesoscale binder-crystal interactions in energetic materials	
Report title: An adaptive numerical methodology for mesoscale binder-crystal interactions and damage propagation in impact loaded energetic materials	

Abstract

The ability to model the stress concentration, strain localization, crack initiation and propagation at mesoscopic length scales of heterogeneous materials such as polymer bonded explosives is critical to preventing undesirable ignitions.

The research conducted in this study addresses the ability to model the strain localization, crack initiation and propagation by using explicit Lagrangian solution of the underlying partial differential equations within domains of interest discretized using finite elements and initially rigid cohesive elements. This approach is superior in its ability to model stress wave propagation excited by rapidly applied loads along model boundaries as it does not suffer from inaccuracies imposed by numerically generated internal impedance boundaries to their propagation.

New criteria for detection of the onset of strain localisation, new algorithms for activation of initially rigid cohesive elements, strain softening, crack initiation and crack propagation have been implemented within in-house software DEST (Discrete Elements Simulation Tools) in order to enable existing and new experimental data to be used to enable further improvements of both the understanding of the underlying physical process as well as thus motivated further improvements of related modelling capabilities.

The developed algorithms are presented alongside benchmarks which confirm their effectiveness.

Distribution: SMG Library (2 hard copies + PDF) Sponsor (PDF)		**Authorised by:**
Date 26/09/17	**Authors** Sascha Knell, Antonio Pellegrino, Nik Petrinic	**Page of pages** 1 of 11

1 Introduction

This report provides a summary of findings obtained during a relatively short (six months long) research effort exerted to advance the fundamental aspects of explicit Lagrangian finite element (FE)-based modelling simulations of the mechanical response of solids subjected to impact loading related to the three-dimensional localised brittle and quasi-brittle fracture at mesoscopic length scale. This project relied entirely upon the resources and facilities available within the Impact Engineering Laboratory of the University of Oxford, an integral part of the Solid Mechanics and Materials Engineering Group within the Department of Engineering Science. The key resource needed to advance the proposed modelling capabilities was DEST (Discrete Element Simulation Tools) software developed by Professor N. Petrinic's research group over the last couple of decades. In addition, the existing experimental data generated previously in the wider research group was used to obtain some fundamental properties of relevant polymeric materials, while a new set of experiments was developed particularly to enable detailed validation of specific modelling methodologies developed and implemented during the course of this project.

The research was motivated by its importance in the context of the sensitivity analysis of heterogeneous energetic (HE) materials, such as polymer-bonded explosives (PBXs), by enabling the modelling of emergence and evolution of "hotspots" or fracture initiation sites as a part of the observed mechanical response of this class of materials. This is inherently related to the chemical composition and the mesoscopic system material structure, which define the distribution, magnitude, concentration and localisation of excited reversible and irreversible thermo-mechanical response mechanisms. Consequently, any sensitivity analysis of HE materials requires accurate prediction of the deformation within the bulk as well as of the relative motion within zones of strain localisations and along interfaces between heterogeneous subdomains, i.e. inert binder and reactive crystals, to understand the initiation and evolution of damage and adiabatic heat induced by rapidly applied impulsive loading.

The simulation methodology underpinning the work proposed in the following section aligns with that employed by Barua and Zhou [4] but aims to employ "extrinsic" (initially rigid) cohesive elements. The choice of an extrinsic formulation is motivated by the fact that, especially for the numerical analysis to provide the understanding of thermo-mechanical response of HE materials subjected to impact loading, it has to be employed at mesoscopic length scales where the explicit modelling of the morphology of materials under consideration, in particular the binder, the crystalline grains and their interfaces, can be conducted. Often, instead of dealing with macroscopic samples, representative volume elements (RVEs) are analysed. Due to the necessity to resolve the highly transient nature of the impact-induced phenomena such as high-frequency waves, explicit time integration algorithms are usually adopted in solutions of the underlying governing partial differential equations, discretised in some manner in both the spatial and temporal domains. In the given context, Eulerian and Lagrangian spatial, predominantly finite element (FE)-based, discretisations are commonly employed.

The Eulerian approach with its temporarily invariant spatial discretisation is particularly suited for problems exhibiting large deformations since, in contrast to the Lagrangian approach in which the discretisation follows the deformation, it does not suffer from reduced precision and a shortened admissible time step in the face of significant distortions. Furthermore, the coupling of the mechanical response to heat transfer and other phenomena, which are usually also modelled in the Eulerian framework, is straightforward. An example for adoption of the Eulerian approach is the work conducted by Rai and Udaykumar [32] (for the method see [14]). The work focuses on the dependence of the ignition behaviour on the morphology, particularly on orientation, size and distributions of voids, of shock-loaded pressed HMX energetic material.

However, imposing specific boundary conditions, simulating damage induced strain localisation, and leading to fracture, fragmentation and multi-body interaction including friction is handled more naturally within the Lagrangian framework. An example is the work of Barua and Zhou [4] in which they presented a computational framework for simulating the mesoscale thermo-mechanical response of PBXs. Their framework makes use of "intrinsic" (initially elastic) cohesive elements embedded between bulk elements to explicitly model the cohesive zone preceding fracture within and between the mesoscopic constituents of the HE material. Subsequent works [2, 3, 5, 15, 16], which build upon this framework, focussed more on the ignition and thermal aspects.

Finally, it should be mentioned that all approaches from the literature referenced above rely on two-dimensional spatial discretisations.

Aligned with the declared motivation and building upon the existing simulation capabilities demonstrated above, this study aims to improve the three-dimensional extrinsic cohesive element formulation developed in [18] explicitly with respect to its ability on to model more accurately localised damage, failure and eventually fracture within heterogeneous materials, such as HE materials. In this context, the ability of the initially rigid cohesive formulation to model the localisation of damage within homogeneous domains of heterogeneous materials, which showed to have potential for improvement in a previous study [17], will be investigated and eventually improved. In particular the investigation will involve the criteria for adaptive activation of cohesive elements and the development of algorithms for the prevention of spurious effects responsible for the aforementioned lack of localisation. Regarding the overall methodology, the impact of time stepping on the localisation behaviour will also be addressed.

The improved methodology is expected to complement the research efforts in the broader field by providing a new platform for modelling coupled phenomena, e.g. by allowing to focus on the thermal effects, i.e. on the "hotspots" in the case of HE materials. Moreover, it should be emphasised here that the proposed methodology is not limited to HE materials. For example, the mesoscale simulation of concrete or ceramics is also a suitable field of application.

2 Modifications of the initially rigid cohesive element formulation

This section presents the modifications developed in the course of the project which aim to improve the specific initially rigid cohesive element formulation outlined in Chapter 2.2, especially with regard to an improved localisation modelling. Specifically, three modifications are proposed: a specialised time step control, an improved CT method for the determination of the tractions underlying the failure initiation and an algorithm for the avoidance of hanging nodes.

2.1 Time step control

In the context of initially rigid cohesive elements, determining an admissible time step via classic stability analysis (as underlying the CFL criterion which is usually used for bulk elements), is rendered impractical by a potentially infinite release stiffness. Additionally, allowing a large softening or, considering the worst case, total decohesion over one time step, may lead to a abrupt unloading of the adjacent bulk elements and consequently oscillations and thus spurious activation of other cohesive elements.

Hence, we propose to limit the time step by restricting the magnitude of the separation, $\|\delta\|_2$, so essentially the softening, to a fraction of the minimum critical separation of the cohesive law according to

$$\delta^e_{\mathrm{adm}} = \beta^e \, \delta^e_{\mathrm{c\,min}}, \quad \text{no sum over } e \tag{3.1}$$

where β^e and $\delta^e_{\mathrm{c\,min}}$ are a reduction factor and the minimum critical separation of the cohesive law, respectively, of Γ^e. In the case of the cohesive law employed in this study, $\delta^e_{\mathrm{c\,min}}$ equals the minimum of δ^e_{cn} and δ^e_{ct}. Since the cohesive law is evaluated at the integration points of the cohesive elements, the positions of which coincide with the positions of the nodes of the inactive elements, the admissible time step is limited by restricting the maximum separation of associate node pairs, $\mathcal{N}^{e-}_k$ and $\mathcal{N}^{e+}_k$, which emerge from the split of aforesaid nodes.

Algorithmically, this is achieved by checking for all associated node pairs (provided a node split occurred) of all cohesive elements Γ^e if for a candidate time step Δt_{cand}, which is set to the admissible time step determined for previously checked bulk and cohesive elements $\Delta t^{(n+1/2)}$, the magnitude of the separation of aforesaid node pairs

$$\Delta\bar{u}_k^e = \left\| \Delta t_{\text{cand}} \left(\Delta\dot{\tilde{\mathbf{u}}}_k^{e\,(n-1/2)} + \frac{1}{2}\left(\Delta t^{(n-1/2)} + \Delta t_{\text{cand}}\right) \Delta\ddot{\tilde{\mathbf{u}}}_k^{e\,(n)} \right) \right\|_2 \tag{3.2}$$

where

$$\Delta\dot{\tilde{\mathbf{u}}}_k^{e\,(n-1/2)} = \dot{\tilde{\mathbf{u}}}_k^{e+\,(n-1/2)} - \dot{\tilde{\mathbf{u}}}_k^{e+\,(n-1/2)} \tag{3.3a}$$

$$\Delta\ddot{\tilde{\mathbf{u}}}_k^{e\,(n-1/2)} = \ddot{\tilde{\mathbf{u}}}_k^{e+\,(n)} - \ddot{\tilde{\mathbf{u}}}_k^{e+\,(n)} \tag{3.3b}$$

satisfies the condition

$$\Delta\bar{u}_k^e \leq \delta_{\text{adm}}^e \tag{3.4}$$

If (3.4) is satisfied, $\Delta t^{(n+1/2)}$ does not have to be reduced. If not, Δt_{cand} is reduced using a bisection scheme in which upper bound $\Delta t_{\text{cand}}^{\text{UB}}$ and lower bound $\Delta t_{\text{cand}}^{\text{LB}}$ are initialised to Δt_{cand} and zero, respectively. The start value $\Delta t_{\text{cand}}^{\text{trial}}$ is set to half of Δt_{cand}. A step of the scheme is given by

$$\Delta\bar{u}_k^{\text{trial}\,e} = \left\| \Delta t_{\text{cand}}^{\text{trial}} \left(\Delta\dot{\tilde{\mathbf{u}}}_k^{e\,(n-1/2)} + \frac{1}{2}\left(\Delta t^{(n-1/2)} + \Delta t_{\text{cand}}^{\text{trial}}\right) \Delta\ddot{\tilde{\mathbf{u}}}_k^{e\,(n)} \right) \right\|_2 \tag{3.5a}$$

$$\left.\begin{array}{lll} \text{If} & \Delta\bar{u}_k^{\text{trial}\,e} > \delta_{\text{adm}}^e & \text{then} \quad \Delta t_{\text{cand}}^{\text{UB}} \\ \text{If} & \Delta\bar{u}_k^{\text{trial}\,e} \leq \delta_{\text{adm}}^e & \text{then} \quad \Delta t_{\text{cand}}^{\text{LB}} \end{array}\right\} = \Delta t_{\text{cand}} = \Delta t_{\text{cand}}^{\text{trial}} \tag{3.5b}$$

$$\Delta t_{\text{cand}}^{\text{trial}} = \frac{1}{2}(\Delta t_{\text{cand}}^{\text{LB}} + \Delta t_{\text{cand}}^{\text{UB}}) \tag{3.5c}$$

$$\epsilon_{\text{rel}} = \left\| \frac{\Delta t_{\text{cand}}^{\text{trial}} - \Delta t_{\text{cand}}}{\Delta t_{\text{cand}}^{\text{trial}}} \right\|_2 \tag{3.5d}$$

where ϵ_{rel} is the relative error. If ϵ_{rel} is smaller than a specified value, in this work 0.001, the scheme is stopped and $\Delta t^{(n+1/2)}$ is set to Δt_{cand}.

The contact algorithm adopted in this study is a penalty contact based upon a symmetric facet/facet interaction, in fact facet/facet overlap. Due to the similarity between this contact formulation and the cohesive elements employed, an additional (or optional) time step control similar to the one given above is applied to the contact, which before relied only on a time step control relying on the half step velocities of the previous time step.

2.2 Improved Cauchy theorem's (CT) based method for determination of interface traction

Although the CT traction determination described in [18] provided good results for the modelling of failure of material interfaces, it exhibits a conceptional flaw. At the instance of a node split, the group of bulk elements which connect to the node under consideration are affected by the nodal mass change. In this study, the failure within homogeneous material domains is considered, i.e. cohesive elements are seeded between all bulk element interfaces which amplifies the effect of element debonding upon the change of nodal mass. To prevent the consequent abrupt change of Cauchy stress within the element, it was proposed that the following modification of its computation is implemented in order to improve the CT traction determination method.

The calculation of the weighted nodal Cauchy stresses is implemented as follows

$$\bar{\boldsymbol{\sigma}}_k = \frac{\bar{\boldsymbol{\alpha}}_k + \sum_{l\,|\,l\in\mathbf{N}_k} \bar{\varphi}_{kl}\,\bar{\boldsymbol{\alpha}}_l}{\bar{\beta}_k + \sum_{l\,|\,l\in\mathbf{N}_k} \bar{\varphi}_{kl}\,\bar{\beta}_l} \tag{3.6}$$

where $\mathbf{N}_k$ is the set of nodal indices of those nodes which are—in the context of node splits—siblings to node $\mathcal{N}_k$.

$$\bar{\varphi}_{kl} = \begin{cases} 1 & \text{initially} \\ \min\left(\bar{\varphi}_{kl}, \left\langle 1 - \dfrac{\Delta\bar{u}_{kl}}{\bar{\delta}_{\mathrm{c}\,k}} \right\rangle\right) & \text{afterwards} \end{cases}, \quad \text{no sum over } k \tag{3.7}$$

is a mitigation factor which tends to zero with increasing

$$\Delta\bar{u}_{kl} = \|\bar{\mathbf{u}}_l - \bar{\mathbf{u}}_k\|_2, \tag{3.8}$$

which corresponds to the distance between $\mathcal{N}_k$ and $\mathcal{N}_l$.

$$\bar{\delta}_{\mathrm{c}\,k} = \left(\min_{e\,|\,\bar{\Gamma}^e \ni \mathcal{N}_m} \delta^e_{\mathrm{c\,min}} \right)\Big|_{t=0}, \quad m = k \,\dot{\vee}\, m \in \mathbf{N}_k \tag{3.9}$$

is the minimum of the critical separations of the cohesive laws of all cohesive elements Γ^e connected to the node $\mathcal{N}_m$ in the initial configuration, i.e., before any node splits occurred. It can be considered as in influence radius of a circle or sphere within which the siblings influence the value of $\bar{\boldsymbol{\sigma}}_k$ of node $\mathcal{N}_k$.

The algorithm for the computation of $\bar{\boldsymbol{\sigma}}_k$ given above is illustrated by the example cases depicted in Figure 3.1. It shows a detail of a two-dimensional FE partition in which one original node has been split into four nodes in consequence of cohesive element activation.

The decision to use $\Delta\bar{u}_{kl}$ and $\delta_{\mathrm{c}\,k}$ to calculate the mitigation factor $\bar{\varphi}_{kl}$ instead of relying on the products of damage values of sequences of active load-bearing cohesive elements, which is seemingly the more natural choice, can be illustrated by case (d). In case of the contributions of Ω_3 and Ω_4 to $\bar{\boldsymbol{\sigma}}_4$ two sequences of cohesive elements exist. The first sequence is Γ_5 and $\bar{\Gamma}_4$ whereas the second consists of $\bar{\Gamma}_7$ and $\bar{\Gamma}_2$. It is unclear how to weight between the two sequences. The situation is even aggravated if the sequences span more than two cohesive elements and more than two sequences exist which is more than probable for tree-dimensional partitions. By contrast, the approach based upon $\Delta\bar{u}_{kl}$ and $\bar{\delta}_{\mathrm{c}\,k}$ avoids the afore-mentioned ambiguities and can be applied to arbitrarily complex as well as three-dimensional cases.

With regard to the implementation, it should be mentioned that if $\bar{\varphi}_{kl}$ equals zero, the index l is removed from $\mathbf{N}_k$. This shortens the calculation of (3.6) and makes the storage and computation of $\bar{\varphi}_{kl}$ and $\Delta\bar{u}_{kl}$ redundant.

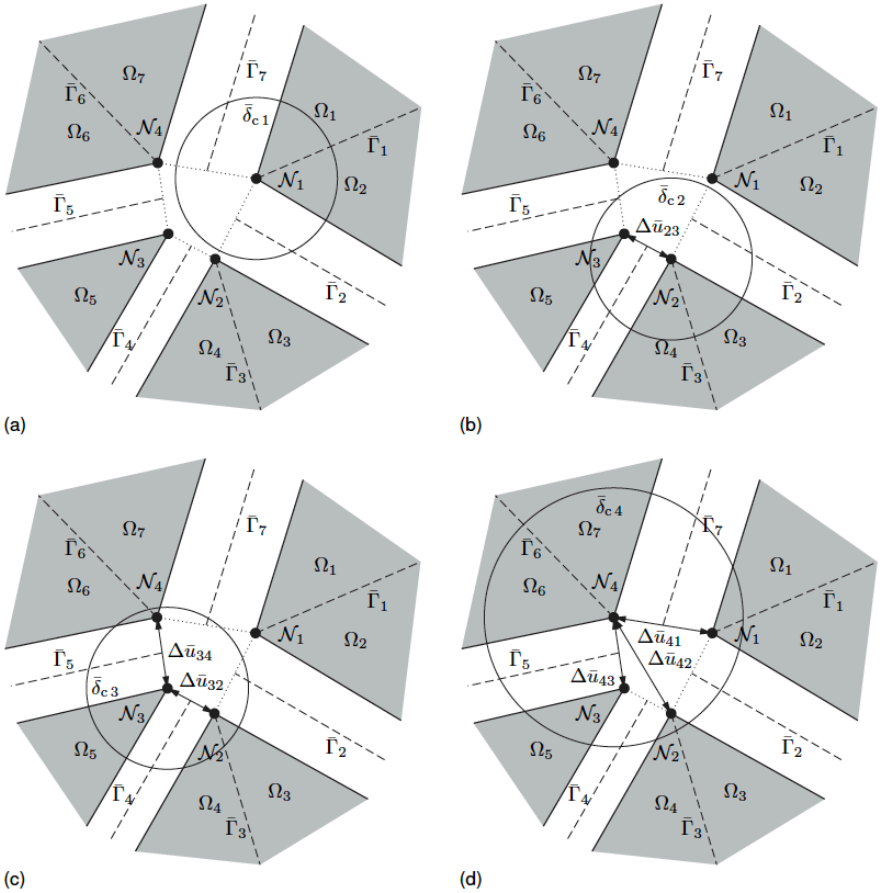

Figure 3.1: Details of a two-dimensional FE partition in which one original node has been split into four nodes in consequence of cohesive element activation, which serve the illustration the improved CT method.

3 Results and discussion

The effectiveness of the modifications of the proposed formulation as well as the overall suitability and limitations of the final formulation will be measured and discussed based on their application to two three-dimensional benchmark problems. In the early stage of the project, it became clear that the simulation of HE materials is not ideal for a comparative analysis of the modifications, which focus on localisation within homogeneous material regions. This is mainly due to the lack of well documented experimental results with an emphasis on the mechanical response within those homogeneous regions. Furthermore, the material data published in the literature governing the localisation behaviour is scarce—especially with regard to different temperature regimes, which are of critical importance for the material class considered.

As an alternative, polymethylmethacrylat (PMMA), a material often used for the validation of cohesive zone approach-based formulations, is employed as the primary benchmark. The "compact compression specimen" (CCS) experiment proposed by Rittel et al. [34] (see also [20, 33]) is used, in which a mode 1-dominated, curved crack within a homogeneous material is induced by impulsive loading with a compression split Hopkinson bar. Despite its widespread adoption as a benchmark problem, the documentation concerning the temporal evolution of the crack trajectory within PMMA is insufficient. The facts that PMMA is readily available and that a suitable experimental setup exists in our laboratory, allowed us to conduct and document the CCS experiment ourselves.

Nevertheless, to demonstrate the applicability of the final formulation within the field which motivated this work, the second benchmark is derived from the simulations of dynamically loaded PBX published by Barua and Zhou [4].

It should be noted, that due to the computational effort resulting from the necessity to spatially and temporarily resolve the evolution of cohesive zones within the 3D simulations of the benchmark problems, only thin slices of the respective specimens can be considered. To avoid buckling, the FE partitions are confined by suitable displacement boundary conditions such that a plain strain-like state is maintained during the simulations.

All FE partitions of the benchmark problems considered were created with Gmsh [13]. ParaWiew was used for the visualisation of the results, all of which were generated with the research group's in-house DE-FE-code DEST.

3.1 Simulation of a generic uniaxial compression experiment

As mentioned at the beginning of this section, the final formulation proposed in this work will be applied to a benchmark problem derived from 2D simulations conducted by Barua and Zhou [4]: the dynamic compression of elastic particulates embedded in a viscoelastic matrix representing reactive crystals enclosed in an inert binder of a PBX. This benchmark serves only the purpose of verification of the general applicability of the final formulation to HE materials and, given the simplified material description adopted, should be considered as generic.

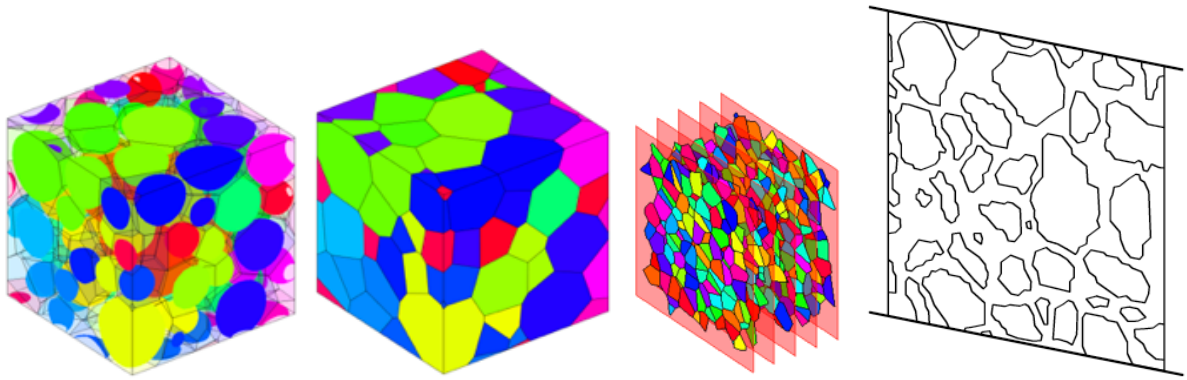

Figure 4.13: Geometry of the PBX representation and the anvil stubs used in the simulation.

Table 4.3: Bulk material parameters for the generic PBX compression benchmark

	Crystals	Anvils		Binder
ρ [g/cm^3]	1.58	4.43	ρ [g/cm^3]	1.28
E [kPa]	2.532 10^7	1.09 10^8	K [kPa]	3.65 10^6
ν	0.25	0.342	G_0 [kPa]	0
c_l	0.1	0.1	c_l	0.1
c_q	1	1	c_q	1
α_CFL	0.8	0.8	α_CFL	0.8

Table 4.4: Relaxation times and shear moduli for a generalised Maxwell model for two temperatures for the binder employed in the generic PBX compression benchmark

cell number i	τ_i [ms] for 19 °C	τ_i [ms] for 0 °C	G_i [kPa]
1	1.5 10^9	2.505 10^{10}	4.169
2	1.5 10^8	2.505 10^9	7.413
3	1.5 10^7	2.505 10^8	1.585 10^1
4	1.5 10^6	2.505 10^7	3.802 10^1
5	1.5 10^5	2.505 10^6	6.761 10^1
6	1.5 10^4	2.505 10^5	8.913 10^1
7	1.5 10^3	2.505 10^4	1.156 10^2
8	1.5 10^2	2.505 10^3	1.422 10^2
9	1.5 10^1	2.505 10^2	1.622 10^2
10	1.5	2.505 10^1	2.218 10^2
11	1.5 10^{-1}	2.505	4.753 10^2
12	1.5 10^{-2}	2.505 10^{-1}	2.618 10^3
13	1.5 10^{-3}	2.505 10^{-2}	1.288 10^4
14	1.5 10^{-4}	2.505 10^{-3}	5.248 10^4
15	1.5 10^{-5}	2.505 10^{-4}	2.239 10^5
16	1.5 10^{-6}	2.505 10^{-5}	4.365 10^5
17	1.5 10^{-7}	2.505 10^{-6}	4.571 10^5
18	1.5 10^{-8}	2.505 10^{-7}	3.467 10^5
19	1.5 10^{-9}	2.505 10^{-8}	2.512 10^5
20	1.5 10^{-10}	2.505 10^{-9}	1.778 10^5
21	1.5 10^{-11}	2.505 10^{-10}	1.175 10^5
22	1.5 10^{-12}	2.505 10^{-11}	7.586 10^4

Table 4.5: Cohesive material parameters variations employed in the generic PBX compression benchmark

	Binder V1	Interface V1	Binder V2	Interface V2
t_cn [kPa]	3.84 10^4	3.5 10^4	3.84 10^4	3.5 10^4
t_ct [kPa]	3.84 10^4	3.5 10^4	7.68 10^4	7 10^4
G_cn [J/m^2]	1.92 10^2	8.085 10^1	1.92 10^2	8.085 10^1
G_ct [J/m^2]	1.92 10^2	8.085 10^1	3.84 10^2	1.617 10^2
η	1	1	1	1
α_coh	2.5 10^{-2}	2.5 10^{-2}	2.5 10^{-2}	2.5 10^{-2}

Table 4.6: Selected variants of the PBX compression simulations conducted

variant	temperature	cohesive parameters
A	19 °C	V1
B	19 °C	V2
C	0 °C	V1
D	0 °C	V2

The three-dimensional geometry used here is shown in Figure 4.13. It is adapted from the upper left quarter of the micrograph displayed in Figure 2 (a) from [5] which is attributed to Siviour et al. [37]. As before, the three-dimensional FE discretisation is based on the extrusion of an unstructured surface mesh and the structured partition of the resulting wedges with three tetrahedrons. The compressive loading of the specimen is realised by geometrically disconnected bottom and top anvil stubs as shown in the figure which are imposed with the respective boundary conditions. Length and height of the specimen are each equally 1.5 mm. A thickness and uniform characteristic element length of 0.005 mm are employed. The total number of tetrahedral bulk elements is 719,946. Inactive cohesive elements are only seeded within the binder and at crystal-binder-interfaces.

All translational degrees of freedom of the bottom nodes of the lower anvil stub are fixed. The top surface of the upper anvil stub is imposed with a vertically acting velocity boundary condition. Initially, the velocity is ramped up linearly over 0.001 ms from 0 m/s to -25 m/s and is kept constant afterwards. Effectively, this corresponds a technical strain rate within the specimen of 16667 1/s.

The bulk material parameters employed are given in Tables 4.3 and 4.4. The data for the reactive HMX crystals, which are assumed to be purely elastic, are taken from [4]. In contrast to the bulk material model employed for the binder in [4], plasticized Estane, deformation-induced temperature changes within the material are neglected in this study. The density of the plasticized Estane is taken from [8]. Its constant bulk modulus K and the parameters for a generalised Maxwell model governing its viscoelastic shear response, the elastic shear modulus G_0, the Maxwell cell relaxation times and shear moduli τ_i and G_i, respectively, are taken from [21]. Here, two constant temperatures are considered, viz. 19 °C and 0 °C. Both temperatures are well above the glass transition temperature of −40 °C of the material [8].

The cohesive material parameters adopted for the binder and the crystal-binder-interfaces are given in Table 4.5. The mode 1 values follow from the critical tractions and separations from [4] which are partially based on the fracture energies determined by Dienes and Kershner [11] and Tan et al. [38] for binder and interface, respectively. Given the considerable shear deformations expected within the binder, an additional set of increased mode 2 parameters, denoted by V2, is adopted in the benchmark simulations.

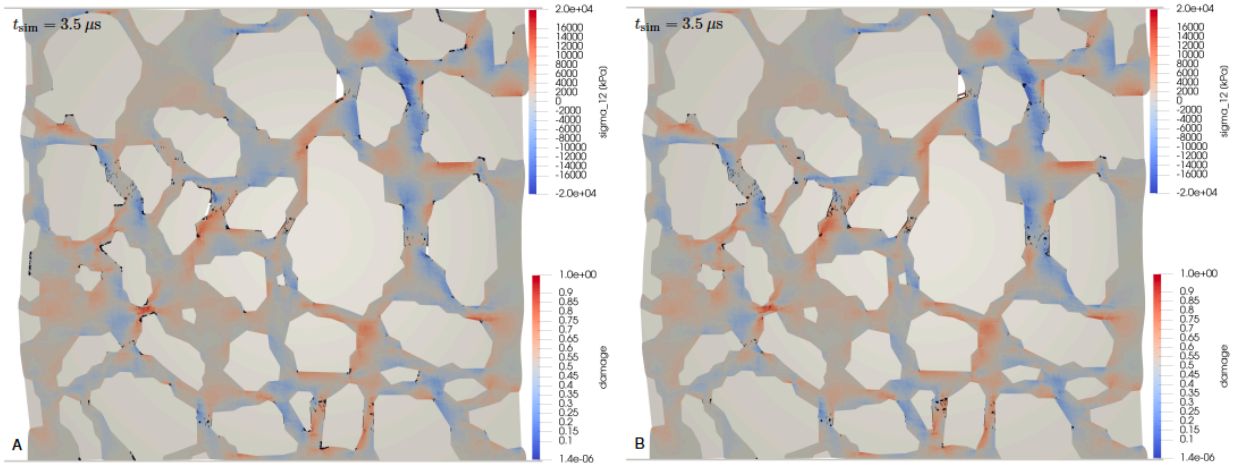

Figure 4.14: In-plane shear stress in the binder and damage in active cohesive elements of the generic PBX compression simulation variants A and B at the end of the simulation interval considered.

In consequence of the two temperatures and the two cohesive material parameter sets adopted, four simulation variants of the generic benchmark problem, as specified in Table 4.6, will be considered in the following. Results of these four variants are depicted in the Figures 4.14 and 4.15. The results attained for the higher temperature, i.e., lower relaxation times, show less active cohesive elements and fracture

surfaces, which are predominately located at the crystal-binder-interfaces, than those for the lower temperature. As expected, the magnitude of shear stress concentrations is also lower for the higher temperature. The variation of the mode 2 parameters has only a minor impact on the results for the higher temperature. In contrast, the impact is significant for the lower temperature. For variant C, the dynamic shear resistance of the binder is so high that clusters of activated cohesive elements can be observed. That these clusters are at least partially a consequence of an activation due to mode 2 failure is strongly supported by the absence of those clusters for variant D. It should be noted that a material model which accounts for a reduction of the relaxation times in consequence of deformation-induced self-heating, as adopted in [4], might alleviate the issue for lower temperatures. Figure 4.16 illustrates another factor which, aside from its general negative impact on the validity of the simulation results, is partially responsible for the occurrence of clusters of active cohesive elements observed. The detail depicted on the right-hand side of the figure shows clearly spurious pressure modes at locations exhibiting high shear stresses (see Figure 4.15). These spurious modes are a consequence of volumetric locking which typically is encountered for (quasi-)incompressible deformations. Therefore, in addition to the fact that spurious pressure modes are problematic for a failure initiation criterion relying on the bulk stresses, volumetric locking effectively and spuriously increases the shear stiffness of the binder. The simulations presented in the literature dealing with Lagrange-based modelling of HE materials referenced at the beginning of this report avoid this issue by relying on two-dimensional structured, cross-triangle FE partitions. It is well known that these special structured partitions do not lock [23] (as long as the partitions remain virtually undeformed). Aside from the aforementioned issues the applicability of the simulation methodology proposed in this study is affirmed by the above results. However, special care is required exploring
the limitations of its application on a case by case basis.

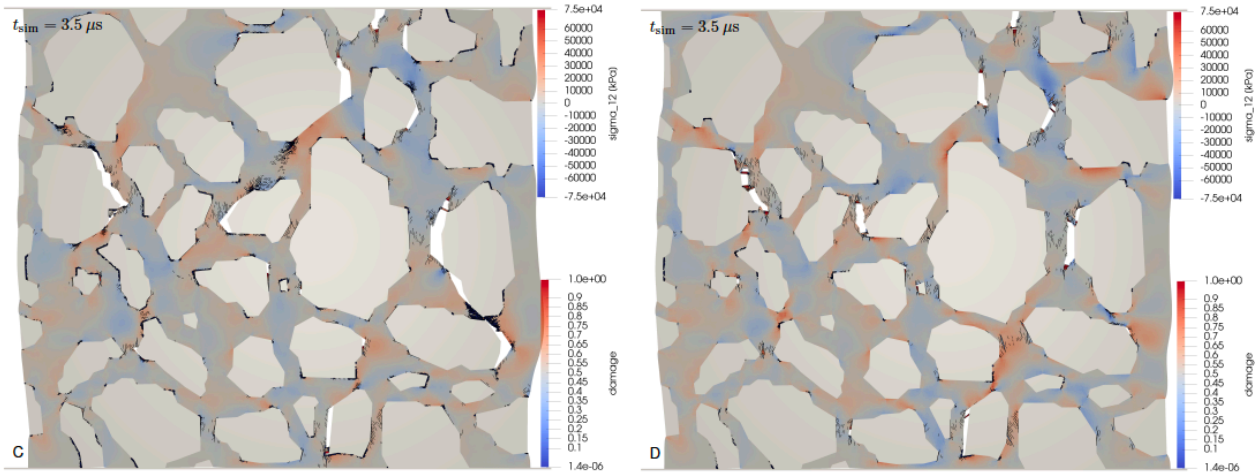

Figure 4.15: In-plane shear stress in the binder and damage in active cohesive elements of the generic PBX compression simulation variants C and D at the end of the simulation interval considered.

4 Conclusions

During the course of this study three modifications of an existing initially rigid cohesive element formulation, which is part of a spatially three-dimensional explicit Lagrangian finite element approach, were proposed with the aim to improve the modelling of localised failure, specifically the avoidance of spurious failure bifurcations, within homogeneous areas of heterogeneous materials.

The first modification of the baseline formulation is a robust time step control for the cohesive elements. A variant of this time step control has also been applied to the symmetric penalty contact adopted. The second modification improved the method for the determination of the tractions upon which the failure initiation is based. The third modification is an algorithm which helps to avoid hanging nodes, i.e., bridging nodes which prevent a continuous opening of an evolving cohesive zone. The three modifications were compared against each other and the baseline formulation by simulation of a "compact compression specimen" (CCS) experiment in which the CCS is impulsively loaded by a split Hopkinson bar. Since data regarding temporal evolution of the crack trajectory is insufficiently documented in the literature, the experiments have been conducted with an PMMA specimen of reduced dimensions using an existing experimental setup. The simulations, which were conducted on thin virtual specimens, due the immense

computational effort involved, exhibited improved results with regard to the localization behaviour for the second and the third modification. The perceived lack of an effect of the enhanced time step control is presumably due the necessity to employ a similar time step control scheme for the contact. Occasionally, cohesive elements bridging the evolving crack were observed if the algorithm for the avoidance of hanging nodes was adopted. A side effect of this algorithm is the increase of the distance for which the cohesive elements can still transmit tractions, which presumably explains the bridging elements. The direct comparison of the results of the experiment and the simulations employing the final methodology, which includes all modifications, showed a remarkably good agreement.

The final formulation was applied to simulate a generic dynamic compression test of elastic particulates enclosed in a viscoelastic matrix representing reactive crystals embedded in an inert binder for two temperatures and two different mode 2 resistances. Here, also thin virtual specimens were considered. The simulations supported the applicability of the method developed in the numerical analysis to HE materials.

5 References

[1] G.I. Barenblatt. The Mathematical Theory of Equilibrium Cracks in Brittle Fracture. Advances in Applied Mechanics, 7:55–129, January 1962.

[2] A. Barua, S. Kim, Y. Horie, and M. Zhou. Ignition criterion for heterogeneous energetic materials based on hotspot size-temperature threshold. Journal of Applied Physics, 113(6):064906, 2013.

[3] Ananda Barua, Seok Pum Kim, Yasuyuki Horie, and Min Zhou. Computational Analysis of Ignition in Heterogeneous Energetic Materials. Materials Science Forum, 767:13–21, 2014.

[4] Ananda Barua and Min Zhou. A Lagrangian framework for analyzing microstructural level response of polymer-bonded explosives. Modelling and Simulation in Materials Science and Engineering, 19(5):055001, 2011.

[5] Ananda Barua and Min Zhou. Computational analysis of temperature rises in microstructures of HMX-Estane PBXs. Computational Mechanics, 52(1):151–159, July 2013.

[6] M.L. Benzeggagh and M. Kenane. Measurement of mixed-mode delamination fracture toughness of unidirectional glass/epoxy composites with mixed-mode bending apparatus. Composites Science and Technology, 56(4):439–449, January 1996.

[7] John C. Brewer and Paul A. Lagace. Quadratic Stress Criterion for Initiation of Delamination. Journal of Composite Materials, 22(12):1141–1155, December 1988.

[8] C.M. Cady, W.R. Blumenthal, G.T. Gray, and D.J. Idar. Mechanical properties of plastic-bonded explosive binder materials as a function of strain-rate and temperature. Polymer Engineering & Science, 46(6):812–819, 2006.

[9] G.T. Camacho and M. Ortiz. Computational modelling of impact damage in brittle materials. International Journal of Solids and Structures, 33(2022):2899–2938, August 1996.

[10] Pedro P. Camanho and Carlos G. Dávila. Mixed-mode decohesion finite elements for the simulation of delamination in composite materials. 2002.

[11] J. K. Dienes and J. D. Kershner. Multiple-shock initiation via statistical crack mechanics. Technical report, Los Alamos National Lab., NM (United States), 1998.

[12] D.S. Dugdale. Yielding of steel sheets containing slits. Journal of the Mechanics and Physics of Solids, 8(2):100–104, May 1960.

[13] Christophe Geuzaine and Jean-François Remacle. Gmsh: A 3-D finite element mesh generator with built-in pre- and post-processing facilities. International Journal for Numerical Methods in Engineering, 79(11):1309–1331, 2009.

[14] A. Kapahi, S. Sambasivan, and H.S. Udaykumar. A three-dimensional sharp interface Cartesian grid method for solving high speed multi-material impact, penetration and fragmentation problems. Journal of Computational Physics, 241:308–332, May 2013.

[15] S. Kim, A. Barua, Y. Horie, and M. Zhou. Ignition probability of polymer-bonded explosives accounting for multiple sources of material stochasticity. Journal of Applied Physics, 115(17):174902, 2014.

[16] Seokpum Kim, Christopher Miller, Yasuyuki Horie, Christopher Molek, Eric Welle, and Min Zhou. Computational prediction of probabilistic ignition threshold of pressed granular octahydro-1,3,5,7-tetranitro-1,2,3,5-tetrazocine (HMX) under shock loading. Journal of Applied Physics, 120(11):115902, 2016.

[17] S. Knell, M. Sauer, O. Millon, and W. Riedel. Mesoscale simulation of concrete spall failure. The European Physical Journal Special Topics, 206(1):139–148, May 2012.

[18] Sascha Knell. A numerical modeling approach for the transient response of solids at the mesoscale. Fraunhofer-Verlag, 2011.

[19] R.P. Kusy and D.T. Turner. Influence of the molecular weight of poly(methyl methacrylate) on fracture morphology in notched tension. Polymer, 18(4):391–402, April 1977.
[20] H. Maigre and D. Rittel. Dynamic fracture detection using the force-displacement reciprocity: application to the compact compression specimen. International Journal of Fracture, 73(1):67–79, August 1995.
[21] E. M. Mas, B. E. Clements, B. Blumenthal, C. M. Cady, G. T. Gray, and C. Liu. A Viscoelastic Model for PBX Binders. AIP Conference Proceedings, 620(1):661–664, 2002.
[22] N. Murphy and A. Ivankovic. The prediction of dynamic fracture evolution in PMMA using a cohesive zone model. Prospects in Fracture Papers from a Conference held to Celebrate the 65th Birthday of Professor J.G. Williams, FRS, FREng Imperial College London, July 2003, 72(6):861–875, April 2005.
[23] J.C. Nagtegaal, D.M. Parks, and J.R. Rice. On numerically accurate finite element solutions in the fully plastic range. Computer Methods in Applied Mechanics and Engineering, 4(2):153–177, September 1974.
[24] M. Nossek, M. Sauer, and K. Thoma. Adaptive Simulation of cohesive interface debonding for crash and impact analyses. In C. A. Motasoares, J. A. C. Martins, H. C. Rodrigues, Jorge A. C. Ambrósio, C. A. B. Pina, C. M. Motasoares, E. B. R. Pereira, and J. Folgado, editors, III European Conference on Computational Mechanics: Solids, Structures and Coupled Problems in Engineering: Book of Abstracts, pages 504–504. Springer Netherlands, Dordrecht, 2006. DOI: 10.1007/1-4020-5370-3_504.
[25] M. Ortiz and A. Pandolfi. Finite-deformation irreversible cohesive elements for threedimensional crack-propagation analysis. International Journal for Numerical Methods in Engineering, 44(9):1267–1282, 1999.
[26] P. A. Klein, J. W. Foulk, E. P. Chen, S. A. Wimmer, and H. Gao. Physics-based Modeling of Brittle Fracture: Cohesive Formulations and the Application of Meshfree Methods. Technical report, United States, December 2000. DOI: 10.2172/772347.
[27] A. Pandolfi and M. Ortiz. Solid modeling aspects of three-dimensional fragmentation. Engineering with Computers, 14(4):287–308, 1998.
[28] A. Pandolfi and M. Ortiz. An Efficient Adaptive Procedure for Three-Dimensional Fragmentation Simulations. Engineering with Computers, 18(2):148–159, 2002.
[29] Katerina D. Papoulia, Chin-Hang Sam, and Stephen A. Vavasis. Time continuity in cohesive finite element modeling. International Journal for Numerical Methods in Engineering, 58(5):679–701, 2003.
[30] Katerina D. Papoulia, Stephen A. Vavasis, and Pritam Ganguly. Spatial convergence of crack nucleation using a cohesive finite-element model on a pinwheel-based mesh. International Journal for Numerical Methods in Engineering, 67(1):1–16, 2006.
[31] Glaucio H. Paulino, Kyoungsoo Park, Waldemar Celes, and Rodrigo Espinha. Adaptive dynamic cohesive fracture simulation using nodal perturbation and edge-swap operators. International Journal for Numerical Methods in Engineering, 84(11):1303–1343, 2010.
[32] Nirmal K. Rai and H. S. Udaykumar. Mesoscale simulation of reactive pressed energetic materials under shock loading. Journal of Applied Physics, 118(24):245905, 2015.
[33] D. Rittel and H. Maigre. An investigation of dynamic crack initiation in PMMA. Mechanics of Materials, 23(3):229–239, July 1996.
[34] D. Rittel, H. Maigre, and H.D. Bui. A new method for dynamic fracture toughness testing. Scripta Metallurgica et Materialia, 26(10):1593–1598, May 1992.
[35] Chin-Hang Sam, Katerina D. Papoulia, and Stephen A. Vavasis. Obtaining initially rigid cohesive finite element models that are temporally convergent. Engineering Fracture Mechanics, 72(14):2247–2267, September 2005.
[36] Chin-Hang Sam, Katerina D. Papoulia, and Stephen A. Vavasis. Erratum to Obtaining initially rigid cohesive finite element models that are temporally convergent [Engineering Fracture Mechanics 72 (2005) 22472267]. Engineering Fracture Mechanics, 73(8):1115, May 2006.
[37] C.R Siviour, P.R Laity, W.G Proud, J.E Field, D Porter, P.D Church, P Gould, and W Huntingdon-Thresher. High strain rate properties of a polymer-bonded sugar: their dependence on applied and internal constraints. Proceedings of the Royal Society A: Mathematical, Physical and Engineering Science, 464(2093):1229, May 2008.
[38] H. Tan, C. Liu, Y. Huang, and P.H. Geubelle. The cohesive law for the particle/matrix interfaces in high explosives. Journal of the Mechanics and Physics of Solids, 53(8):1892–1917, August 2005.
[39] J. G. Williams. Fracture Mechanics of Polymers. Ellis Horwood, 1984.
[40] X.-P. Xu and A. Needleman. Numerical simulations of fast crack growth in brittle solids. Journal of the Mechanics and Physics of Solids, 42(9):1397–1434, September 1994.
[41] Fenghua Zhou, Jean-François Molinari, and Tadashi Shioya. A rate-dependent cohesive model for simulating dynamic crack propagation in brittle materials. Engineering Fracture Mechanics, 72(9):1383–1410, June 2005.